Article

Age-Dependent Molecular and Metabolic Rewiring Leading to Wound-Induced Blackening in Cut Carrots

Katie Shulz , Gabriela Machaj , Paul Knox , Robert Hancock , Susan R Verrall , Risto Korpinen , Pekka Saranpaa , Anna Happonen , Barbara Karpinska , Christine Helen Foyer *

Posted Date: 5 June 2023

doi: 10.20944/preprints202306.0225.v1

Keywords: Auxin; cell wall composition; chlorogenic acid; lignin; pectin; post harvest wounding; tap roots

Article

Age-Dependent Molecular and Metabolic Rewiring Leading to Wound-Induced Blackening in Cut Carrots

Katie Schulz [1], Gabriela Machaj [2], Paul Knox [1], Robert D. Hancock [3], Susan R. Verrall [4], Risto Korpinen [5], Pekka Saranpää [5], Anna Kärkönen [5], Barbara Karpinska [6] and Christine H. Foyer [6]

[1] Centre for Plant Sciences, Faculty of Biological Sciences, University of Leeds, Leeds, LS2 9JT, United Kingdom
[2] Department of Plant Biology and Biotechnology, University of Agriculture in Krakow, 31-120 Krakow, Poland; currentl affiliation: Laboratory of Bioinformatics and Genome Biology, Faculty of Biochemistry, Biophysics and Biotechnology, Jagiellonian University, Kraków 30-387, Poland
[3] Cell and Molecular Sciences, The James Hutton Institute, Invergowrie, Dundee, DD2 5DA. United Kingdom
[4] Ecological Sciences, The James Hutton Institute, Invergowrie, Dundee, DD2 1BE, United Kingdom
[5] Natural Resources Institute Finland, Production Systems, Latokartanonkaari 9, 00790 Helsinki, Finland
[6] School of Biosciences, College of Life and Environmental Sciences, University of Birmingham, Edgbaston, B15 2TT, United Kingdom
* Correspondence: C.H.Foyer@bham.ac.uk

Abstract: The blackening of cut carrots decreases their shelf life and causes severe economic losses but the molecular and metabolic mechanisms that underpin this phenomenon remain poorly characterized. Studies were therefore undertaken to determine the molecular and metabolic causes of the blackening. The susceptibility of blackening was dependent on the period of time that the crop was stored underground prior to harvest. The structure of the cell walls in the black regions was substantially changed compared to the orange regions. The black regions of carrot batons had decreased immunodetection of xyloglucan, HG-pectin, RG-I pectin, galactan and arabinan but had higher levels of lignin and phenolic compounds compared to the orange regions. Transcript profiling analysis revealed that phytohormone signalling processes were activated in the black regions. Transcripts associated with auxin signalling and ethylene-responsive transcription factors were increased in the black regions. In contrast, the levels of transcripts encoding proteins associated with secondary metabolism were decreased in the black regions. These findings implicate ethylene and auxin-related processes in the control of the primary to secondary metabolism shift that results in lignification and cell wall disruption that underpin the blackening process.

Keywords: Auxin; cell wall composition; metabolome; transcriptome; post harvest wounding

1. Introduction

Post-harvest discoloration of fruits and vegetables, which seriously affect flavour and economic value, is a common problem in the food production industry and a major contributor to food wastage. Many factors such as bruising, wounding, herbivory and diseases can contribute to discoloration [1]. Discoloured foods are frequently discarded because of poor customer acceptance of such defects. The disruption of intracellular compartmentation caused by mechanical damage during harvesting, processing or transport causes release of the plastid-localized enzyme polyphenol oxidase (PPO), which can then interact with vacuolar substrates to produce o-quinones, which in turn polymerize to ultimately produce high molecular weight black and brown pigments that are generically called melanin [2-4]. Melanins are toxic and provide resistance to insects and pests as well as give some additional mechanical strength to tissues such as seed shells [4]. Enzymatic browning is a common cause of the discolouration seen in root vegetables [5].

 doi:10.20944/preprints202306.0225.v1

The hardness of vegetables such as carrots is determined by cell walls. Destruction of the internal structure of the cell wall is usually the major reason for softening. The expression of genes regulating the dissociation of the intercellular cell wall layer in fruits, together with the degradation of pectin, and the disintegration of fibrous materials lead to successive disintegration and destruction of cell organelles. Pectin is a main component of primary cell walls and plays an important role in plant development and defence [6]. The pectin backbone is mainly comprised of galacturonic acid, and the two most common pectic polysaccharides are homogalacturonan (HG) and rhamnogalacturonan-I (RG-I; 7]/ Microbial pathogens release cell wall degrading enzymes that loosen the structure of the wall [8]. Plants also produce these enzymes, which are essential for modifying pectin during plant growth and development [9,10]. Pectin is degraded by a variety of enzymes, including polygalacturonases, pectin methylesterases, pectin lyases and pectate lyases Lyases are enzymes that cleave glycosidic bonds specifically in homogalacturonan and rhamnogalacturonan regions [9]. These pectin degrading enzymes become increasingly active after harvest, when the fruits ripen [11]. Pectin degradation produces signals that trigger plant defence responses [12]. Cell wall rigidity is enhanced by lignin. This complex phenolic polymer is associated with all cell walls. Lignin synthesis starts in the cell corners and middle lamella, and thereafter continues through primary cell wall and then proceeds into the secondary cell wall. The concentration of lignin is highest in the middle lamella and primary cell wall, forming an important barrier to pests and pathogens as well as increasing the mechanical strength of the wall [13] Increased lignification is part of the plant defence response to abiotic and biotic stresses [14-16]

Carrots are one of the most important vegetable crops globally. Carrot tap roots are regularly stored underground in the growing fields throughout the United Kingdom for up to 12 months, with each field harvested, as required. Once harvested, carrots can be processed into batons, which are cut roughly into ~7 cm long sections and packaged. Over the last 10 years, a previously unknown and financially crippling blackening phenomenon has been observed in cut carrots that are harvested towards the end of the storage year. The highest level of blackening occurs either on the day of processing (day 0) or the following day (day 1) but the likelihood of blackening is not predictable, often occurring only on supermarket shelves. Little is known about the carrot blackening process and its causes are unknown. While loss of membrane integrity may be a factor in blackening, this is not a rapid process in cut carrots because the black regions can appear throughout the 72h following processing. This latency period in the formation of black regions may be linked to an activation of secondary metabolism and PPO activity following mechanical wounding during processing. Wounding leads to an increase in the accumulation of reactive oxygen species (ROS) and changes in low molecular weight antioxidants and antioxidant enzymes. An enhanced breakdown of the major low molecular weight antioxidant, vitamin C (ascorbate), which produces metabolites such as threonic acid, as a result of wounding could contribute to non-enzymatic blackening in carrots as it does in apples [17]. The following studies were therefore undertaken in order to determine the molecular and metabolic processes that underpin the blackening phenomenon. This information is essential to understand the blackening process and how it is regulated, so that methods of delaying or preventing the blackening can be devised and so reduce unnecessary wastage of food and resources.

2. Materials and Methods

2.1. Plant Materials

Carrots (*Daucus carota* variety 'Nairobi') were harvested from commercial fields and processed in the factories of Kettle Produce Ltd, who provided samples of cut carrot batons over a three-year period. Black and orange samples were harvested from batons from the same batches, together with samples from the border regions between the black and orange tissues. In all cases, samples were harvested and compared from the carrots originating from the same field, grower and date of harvest.

 doi:10.20944/preprints202306.0225.v1

2.2. Cell Wall Analyses

Sample Preparation. Orange and black carrot samples were cut into 1 cm^2 sections and fixed in a PEM buffer (50 mM Pipes, 5 mM EGTA, 5 mM $MgSO_4$, pH 6.9) containing 4% paraformaldehyde for 1 h. Fixed samples were washed twice in 1x PBS for 10 min each time and then dehydrated using increasing concentrations of ethanol (30%, 50%, 70%, 90% and 100%) for 30 min each at 4°C. Samples were warmed to 37°C and incubated overnight at 37°C in 1:1 Steedman's wax and 100% ethanol, followed by two changes of 100% wax for 1 h at 37°C. The samples were positioned in moulds, and wax poured into the moulds until a convex surface was visible, which then set overnight at room temperature. The moulds were chilled for 10 min before samples were cut into 12 µm sections (Microm HM-325 microtome) and placed onto polysine-coated glass slides (VWR International, Leuven, Belgium). The sections were dewaxed and rehydrated using decreasing concentrations of ethanol (3x 97%, 90%, 50%, water) for 10 min each, followed by 1.5 h in water. Microscope sections were then dried.

2.3. Immunolabeling and Fluorescence Imaging and Processing

In this study, the following rat monoclonal antibodies (MAbs) were used: LM25 which binds to xyloglucan [18], LM5 which binds to pectic galactan [19], LM6 to pectic arabinan [20], LM19 to unesterified pectic HG [21], JIM7 to partially methyl-esterified pectic HG [21] and LM20 to highly methyl-esterified pectic HG [21].

Microscope slides containing sections of orange and black carrot tissue were incubated in 5% (w/v) milk protein/PBS for 30 min and rinsed with 1x PBS. Monoclonal primary antibodies (1 in 5 dilution) in 5% (w/v) milk protein/PBS were applied and incubated for 90 min. Sections were washed with 1x PBS three times for 5 min. Secondary antibodies (rabbit anti-rat IgG-fluorescein isothiocyanate (FITC) (Sigma, UK)) were added (1 in 100 dilution) in 5% (w/v) milk protein/PBS and incubated for 60 min in the dark. Sections were washed with 1x PBS three times for 5 min. To prevent interference of background autofluorescence, sections were stained with 0.1% Toluidine Blue O (pH 5.5 in 0.2 M sodium phosphate buffer) for 5 min and excess dye washed off. Sections were mounted in Citifluor AF1 to decrease photobleaching. Slides were viewed with an Olympus fluorescence microscope (Olympus BX61, Canada) and images captured using a Hamamatsu ORCA285 camera (Hamamatsu City, Japan) and Volocity software (Perkin Elmer, UK).

Extracting and Measuring Lignin

Sample Preparation. Orange and black regions in carrot taproots were separated, dried at 60°C and stored in darkness until analyzed. Tissue samples were ground to a fine powder using a Retch ball mill (Retsch MM400, Hann, Germany; 50 ml grinding jars with one metal ball, frequency 30 s^{-1}). The tissue was ground in 30 second intervals 4 times to prevent heating. The extractive-free alcohol-insoluble residue (AIR) was prepared by extracting the sample 8 times with 70% (v/v) ethanol and 3 times with 100% acetone in a 25°C sonicating water bath (30 min incubation time for each extraction with regular mixing). The ratio was 140 mg plant tissue: 14 ml solvent (70% ethanol, acetone). Samples were centrifuged (4000 rpm, 10 mins) before each solvent change and the pellet mixed to the solvent by vortexing. The AIR was dried in a vacuum oven overnight at 60°C.

Lignin was quantified using an acetyl bromide (AcBr) assay [22], as modified by Kärkönen et al., [23]. Five mg of AIR and 5 ml of AcBr reagent (20% AcBr (v/v) in glacial acetic acid) were mixed and incubated at 50°C in a heat block for 3 h with mixing by vortex every 15 mins. AcBr reagent (5 ml) was added to an empty tube as a blank. Samples were cooled in an ice bath for 5 min, then 1.0 ml of the sample mixture was transferred to a 10-ml volumetric flask containing 2.4 ml of glacial acetic acid and 1 ml of 2 M NaOH. After gentle inversion, 0.1 ml of 7.5 M hydroxylamine-HCl was added and then the solution brought to 10 ml using glacial acetic acid. A Shimadzu UV-2401 spectrophotometer (Shimadzu Corp., Kyoto, Japan) was used to measure the absorbance of the sample at 280 nm against a blank that was treated similarly as the samples. Lignin content was calculated using following equation: Lignin% = 100(As – Ab)V/aW [As, absorbance of sample; Ab,

 doi:10.20944/preprints202306.0225.v1

absorbance of blank; V, volume of solution; a, absorptivity of a lignin standard (Klason lignin from spruce xylem, average from two samples 23.087 l g^{-1} cm^{-1}); W, weight of sample]. Five measurements were done from the orange and four from the blackened samples.

2.4. Non-cellulosic Carbohydrate Content

Non-cellulosic carbohydrate analysis was carried out according to Sundberg et al. (1996) using acid methanolysis/gas chromatography (GC)/flame ionization detector (FID). AIR was prepared as described above. Calibration solution contained 0.1 mg/mL of arabinose (Ara), glucose (Glc), glucuronic acid (GlcA), galactose (Gal), galacturonic acid (GalA), 4-O-methyl glucuronic acid (4-O-Me-GlcA), mannose (Man), rhamnose (Rha) and xylose (Xyl) in methanol. AIR (4 mg) prepared from ground carrots was placed in a pear-shaped, pressure resistant flask. One ml calibration solution was dried by evaporation and treated the same way as the carrot samples. Two ml of 2 M solution of HCl in anhydrous MeOH was added and incubated for 5 h at 105°C. Once at room temperature, the solution was neutralized with 80 µl pyridine and shaken well. . An internal standard (4.0 ml) containing 0.1 mg/ml resorcinol in methanol was added and the flask shaken again. A 1-ml aliquot of the solution was evaporated using N_2 gas. A solution containing 70 µl trimethylsilyl chloride (TMCS), 150 µl hexamethyl disilazane (HMDS) and 120 µl pyridine was used to silylate the dried sample at room temperature overnight. Samples were analysed using GC/FID (Shimadzu GC-2010, Kyoto, Japan) with a HP-1 Column (25 m x 0.2 mm I.d., film thickness 0.11 µm). The temperature profile was as follows: 100°C -> 175°C, 4°C/min, 175°C -> 290°C, 12°C/min. The temperature of the injector was 260°C and the temperature of the detector was 290°C. Correction factors were used to calculate the non-cellulosic carbohydrate content; Man, Glc and Gal 0.9, Ara and Xyl 0.88, Rha 0.89, GlcA, GalA and 4-O-Me-GlcA 0.91. Two replicates were used in all analyses.

2.5. Metabolite profiling

Gas chromatography/mass spectrometry (GC/MS) and high-performance liquid chromatography (HPLC) were performed on samples extracted from the orange regions, black regions and the 'border' regions that were immediately adjacent to the black regions. In addition, HPLC analysis was used to identify and quantify carotenoids. In total, seventeen independent biological replicates were identified using the GC/MS approach. Eight independent biological replicates were analysed using the HPLC/MS and HPLC approaches. The major peaks present on the chromatograms obtained by MS were identified on the basis of parent and fragment ion masses present in the mass spectrum of each metabolite. Metabolite profiles were compared by a one-way ANOVA using carrot blackening as the single factor. A total of 64 metabolites were found to be significantly different.

2.6. RNA sequencing (RNA-seq)

RNA was extracted from the orange regions (CT), black regions (B), and the 'border' regions (M) (immediately adjacent to the black regions) using a CTAB method [24] combined with a RNA Clean & Concentrator™ kit (Zymo Research, USA) as described by the manufacturer. Three biological replicates per region were used. The quality and quantity of RNA were determined using NanoDrop ND-1000 (Thermo Fisher Scientific) and gel electrophoresis. Illumina-compatible sequencing libraries were prepared using the Illumina TruSeq Stranded Total RNA-with Ribo-Zero Plant kit. The libraries were checked for adaptor dimers and the insert size on a Tapestation (Agilent) and quantified using the Qubit system, before creating an equimolar pool of libraries. Libraries were sequenced in SE75 (single end mode, 75 bp) using NextSeq 500 (Illumina; San Diego, CA, USA) next-generation sequencing platform.

2.7. RNA-seq Data Analysis

Sequence data were quality-checked using FastQC software followed by quality and adapters trimming in Cutadapt software. Reads trimmed to fewer than 30 nucleotides were discarded. Reads

Preprints (www.preprints.org) | NOT PEER-REVIEWED | Posted: 5 June 2023 doi:10.20944/preprints202306.0225.v1

were aligned to a *Daucus carota* subsp. *sativus* reference genome ASM162521v1 ([26]; Genebank: GCF_001625215.1) using a STAR aligner [26]. The resulting alignments were checked for quality using QualiMap software [27] and Picard tools. Picard was also used to mark PCR/Optical duplicate alignments. Bioconductor R package RSubread [28] was used to extract raw counts per transcript. Differential expression analysis (DEA) was conducted in DeSeq2 [29] R package. The *p*-value was adjusted using the Benjamini-Hotchberg method. Differentially expressed transcripts were identified as those with an adjusted *p*-value of less than 0.05 (Supplemental Table S1). Analysis of Gene Ontology terms were made in Cytoscape with ClueGO v.2.5.7 [30] plug-in based on the functional annotation of all carrot genes provided by Machaj and Grzebelus [31]. Significant (p_{adj}<0.1) terms were visualized in R ggplot2 package [33]. Original data can be fould in the repository Sequence Read Archive (SRA) of the National Center for Biotechnology Information (NCBI) under the project number PRJNA966197 and submission number SUB13217137.

3. Results

3.1. Susceptibility to Blackening Increases with the Time of Storage Prior to Harvest

Processed carrot batons (Figure 1 A and B) and transverse slices (C and D) show a susceptibility to blackening that was was greatest in the batches of carrots that had been stored underground for long periods before harvest (Figure 1E). Carrots harvested at or after 430 days of storage showed at least double the level of blackening after processing observed at any other age range. Carrots that had been stored for less than 161 days showed no blackening after processing (Figure 1E). Hence, the propensity to show processing-induced blackening increased with the age of the carrots.

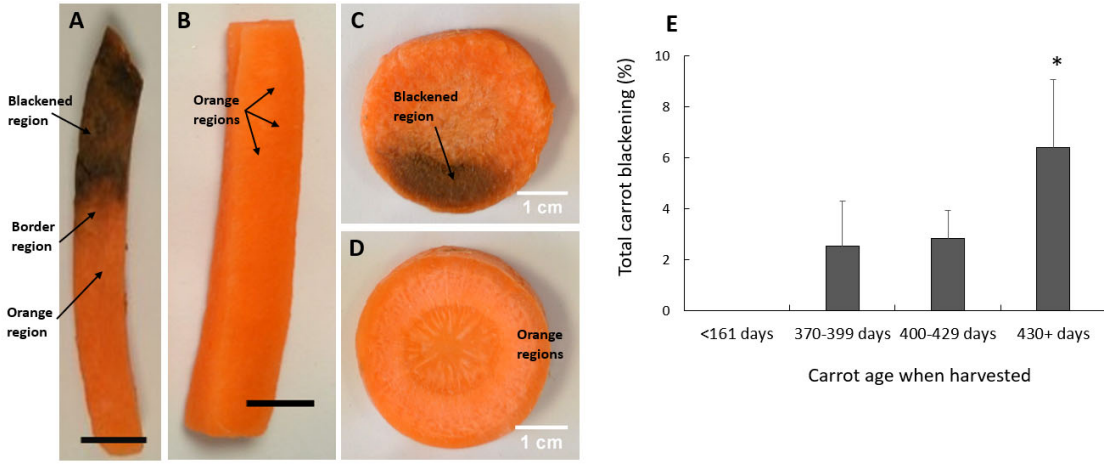

Figure 1. Orange and blackened carrots. Carrot batons (A and B) and transverse slices (C and D). Labelled carrot regions showing orange regions from non-blackened carrots (B and D), orange regions from blackened samples, blackened regions and border regions (A and C). (E) Carrot age at harvesting time. Significant differences were calculated by student t-test. * shows $p \leq 0.05$ and error bars represent SE± . bar = 1 cm.

3.2. Black Region Cells Are Distinct from Orange Region Cells under Bright Field Microscopy

Orange and black carrot sections were viewed with a light microscope. Although the bright field images were taken with the same lighting and camera settings, it was more difficult to distinguish the cell walls of the orange rgions than the black regions at the same settings (Figure 2 A). The cells in the black regions of the batons were significantly smaller than the cells in the orange regions. Discolouration, accompanied by an accumulation of dense material, was observed throughout the cells in the black regions (Figure 2 B, C).

Preprints (www.preprints.org) | NOT PEER-REVIEWED | Posted: 5 June 2023 doi:10.20944/preprints202306.0225.v1

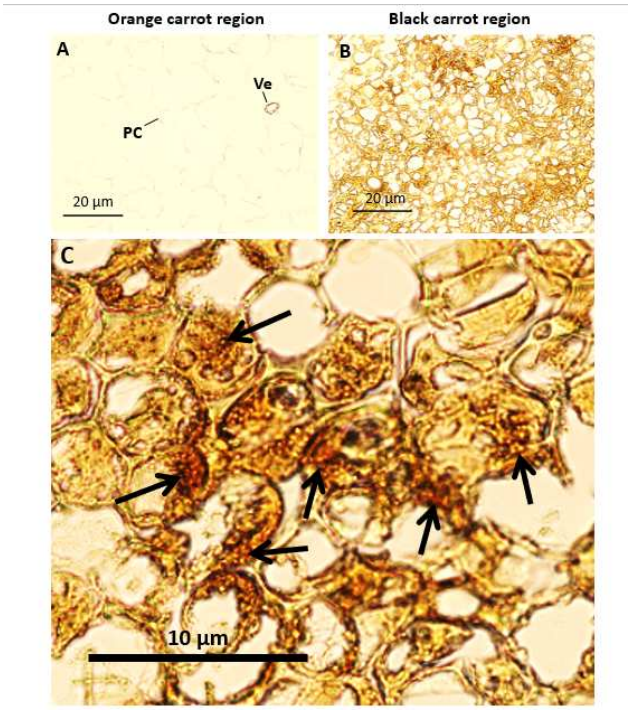

Figure 2. Representative images of orange and black carrot regions. Images were taken of 12 µm carrot sections under the same microscope settings; orange carrot region (A) and black carrot regions (B, C). Arrows indicate areas of carrot blackening. Scale bars = 10 µm and 20 µm.

3.3. Orange and Black Regions of Carrot Batons Have Differing Cell Wall Polysaccharides Profiles

Monoclonal antibodies that bind to xyloglucan (LM25), HG-pectin (LM20, LM19, JIM7) or RG-I pectin (LM5, LM6) were used to gain insight into the polysaccharide content and composition of the cell walls of the black and orange regions of carrot batons. LM26, which binds to a branched pectic galactan epitope of RG-I, was used as a negative control antibody for the immunolabelling technique because it did not bind to the carrot tissue. The cell walls in the black regions of the carrot batons had decreased detection of xyloglucan (Figure 3 F, H) compared to the orange regions (Figure 3 B, D).

Preprints (www.preprints.org) | NOT PEER-REVIEWED | Posted: 5 June 2023 doi:10.20944/preprints202306.0225.v1

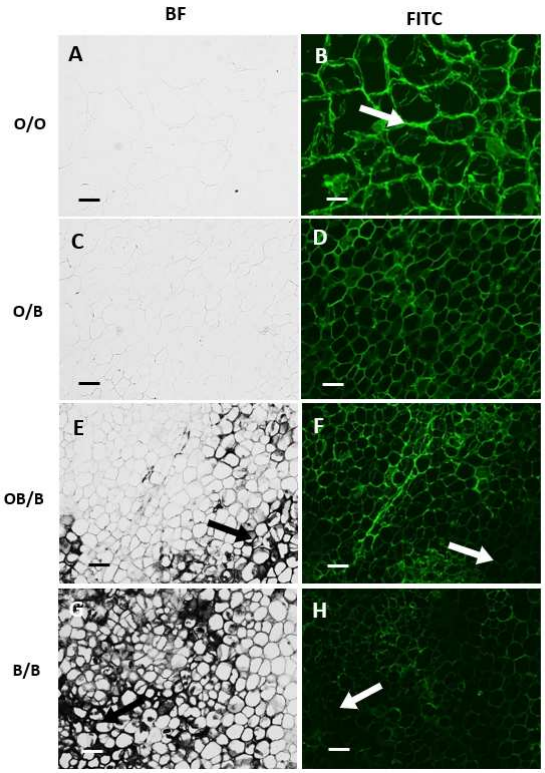

Figure 3. Indirect immunofluorescence detection of the xyloglucan in transverse sections of carrot batons after pectate lyase treatment to remove pectic homogalacturonan. Images showing different carrot sections: orange carrot baton O/O (A, B), orange region on a blackened baton O/B (C, D) tissue directly bordering the black region OB/B (E, F) and the black region B/B (G, H). BF and FITC mean bright field and fluorescence channel, respectively.Corresponding immunofluorescence images for LM25 xyloglucan. Scale bar = 10 μm. 10x magnification. Exposure times: BF = 0.045 s, FITC = 0.15 s. Arrows indicating clear areas of carrot blackening.

The orange and black /orange border regions of the black batons contained significant amounts of detectable pectic HG at all levels of esterification (Figure 4 F, G, N, O, V, W) compared to the orange batons (Figure 4 E, M, U). The black regions had greatly decreased levels of detected pectic HG compared to all other regions (Figure 4 H, P, X). Interestingly, these differences in the detection of the pectic HG epitopes between orange, black and border carrot regions were most clear for the methyl-ester containing epitope of JIM7 and LM20.

Preprints (www.preprints.org) | NOT PEER-REVIEWED | Posted: 5 June 2023 doi:10.20944/preprints202306.0225.v1

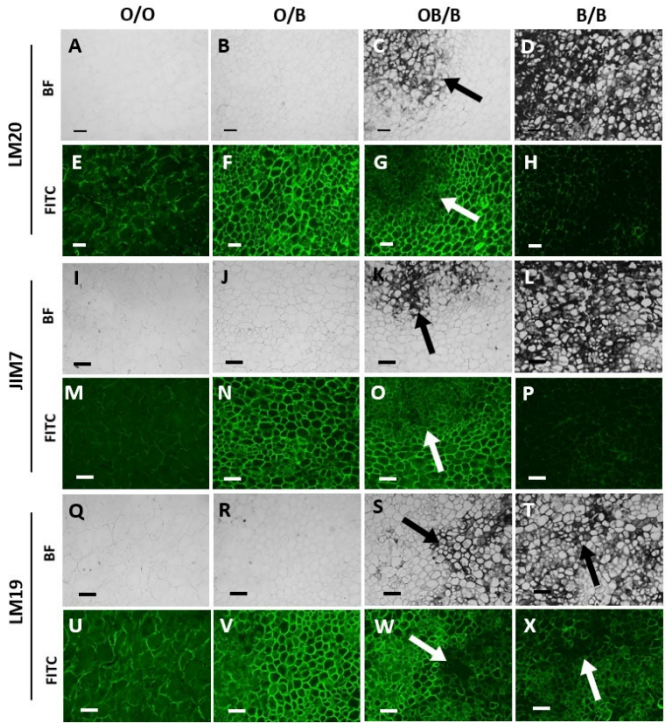

Figure 4. Indirect immunofluorescence detection of pectic HG in transverse sections of orange and blackened carrot batons. Images showing tissue of an orange carrot baton O/O (A, E, I, M, Q, U), orange region on a blackened baton O/B (B, F, J, N, R, V), tissue directly bordering the black region OB/B (C, G, O, S, W), and the black region B/B (D, H, L, P, T, X). BF and FITC mean bright field and fluorescence channel, respectively. Corresponding immunofluorescence images taken in the FITC channel generated with monoclonal antibodies binding to de-esterified pectin (LM19), methyl-esterified pectin (JIM7) and highly esterified pectin (LM20). Scale bar = 10 µm. 10x magnification. LM20 and JIM7 exposure times: BF = 0.011 s, FITC = 0.15 s. LM19 exposure times: BF = 0.011 s, FITC = 0.2 s. Arrows indicating areas of carrot blackening.

LM5 and LM6 were used to detect galactan and arabinan, which are common side chains of RG-I. These RG-I pectin side chains were detected in orange batons (Figure 5 B, D), with decreased amounts in the orange and border regions of the black carrot sections (Figure 5 F, H, J, L). Cell walls in the black regions showed the lowest detection of the LM5 and LM6 epitopes (Figure 5 N, P).

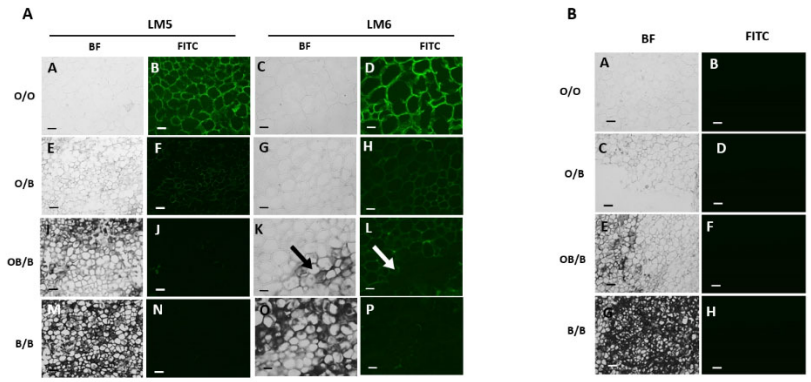

Figure 5. Indirect immunofluorescence detection of pectic RG-I in transverse sections of orange and blackened carrot batons. Images showing tissue of an orange carrot baton O/O; 5A (A, B, C, D) and 5B (A, B), orange region on a blackened baton O/B: 5A (E, F, G, H) and 5B (C, D) tissue directly bordering the black region OB/B 5A (I, J, K, L) and 5B (E, F) and the black region B/B; 5A (M, N, O, P)

Preprints (www.preprints.org) | NOT PEER-REVIEWED | Posted: 5 June 2023 doi:10.20944/preprints202306.0225.v1

and 5B (G, H). BF and FITC mean bright field and fluorescence channel, respectively. Corresponding immunofluorescence images taken in the FITC channel generated with monoclonal antibodies binding to (1-4)-β-galactan (LM5) and (1-5)-α-L-arabinan (LM6). Scale bar = 10 μm. LM5 images are at 10x magnification. Exposure times: BF = 0.045 s, FITC = 0.3 s. LM6 images are at 20x magnification. Exposure times: BF = 0.1 s, FITC = 0.8 s. Arrows indicating clear areas of carrot blackening.

Non-cellulosic cell wall carbohydrate analysis conducted by acid methanolysis/GC gave similar results as immunohistochemistry. Levels of galacturonic acid, the main backbone sugar moiety in pectins, were decreased in black batons compared to orange batons (Supplemental Figure S1A). There were no significant differences in the levels of other non-cellulosic sugars in the orange and black tissues.

3.4. Transcriptome Reprogramming Occurs in Black Regions

Large numbers of transcripts were differentially expressed in the black and border regions compared to the orange regions of the cut carrots (Figure 6).

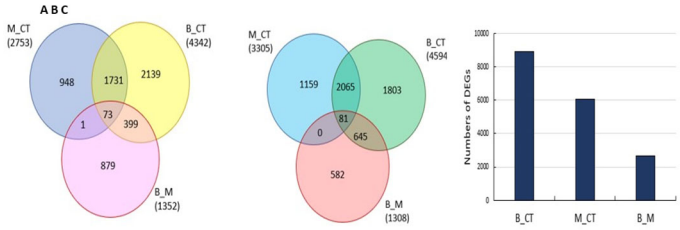

Figure 6. Comparisons of the numbers of differentially expressed genes (Venn diagrams, A, B) and total numbers in the black and border regions compared to the orange regions of the cut carrots (A) Up-regulated DEGs ($\log_2$(FC) ≥ 1), (B) down-regulated DEGs, ($\log_2$(FC) ≤ -1) and (C) number of total DEGs. DESeq2 was used to determine differentially expressed sequences and the *p*-values were corrected for multiple testing using the Benjamini and Hochberg method (*padj.* ≤ 0.05). B_CT blackened *vs* control, M_CT border carrot region *vs* control, and B_M blackened *vs* border regions.

Significant variations in the numbers of differentially expressed genes (DEGs; Supplemental Figure S2A) were observed in the black and border regions compared to the orange regions (Supplemental Figure S2B). KEGG enrichment analysis of comparisions (Supplemental Figure 3) revealed that transcripts encoding many metabolic processes and pathways, such as phenylpropanoid biosynthesis, TCA cycle, cysteine and glutahione metabolism, glycolyis and gluconegenesis, were decreased in abundance in the border and black in regions compared to the orange control tissue. However, some ontology groups, for example, cellular response to auxin stimulus, photosynthesis and starch metabolism were eriched in the black in regions compared to the orange control tissue (Supplemental Figure S4A, B). Enrichment in transcripts acssociated with photosynthesis, carotenoid metabolism and starch metabolism was most pronounced in the border regions compared to the black regions controls (Supplemental Figure S5).

Transcripts associated with tyrosine metabolism including PPO genes (LOC108206452, LOC108192978, LOC108220626, LOC108206527) were significantly decreased in the black and border regions (Supplemental Figure S6). A large number of transcripts encoding proteins involved in the phenylpropanoid pathway were less abundant in the black and border regions than in the orange controls.

A number of transcripts increased in the black regions compared to the orange controls encode phytohormone signalling pathway components (Supplemental Figure S6). For example, auxin-

Preprints (www.preprints.org) | NOT PEER-REVIEWED | Posted: 5 June 2023 doi:10.20944/preprints202306.0225.v1

responsive protein IAA26 was in the list of transcripts that were most significantly increased in the black regions compared to the orange controls (Figure 7, Supplemental Figure S6). In addition, transcripts associated with strigolactone and ethylene signalling were also highly expressed in the black regions (Supplemental Figure S7). (Interestingly, a gene encoding one polygalacturonase, which is the major enzyme responsible for pectin disassembly during fruit ripening, was highly induced in the black regions.

The levels of large numbers of transcripts encoding transcription factors that were changed in the black and border regions relative to the orange regions (Supplemental Figure S8) including members of the WRKY, bHLH (B), ERF, TCP, MYB and GATA families. However, only one transcript associated with hormone functions appears in the list of transcripts that were most decreased in the black regions compared to the orange controls, the (Figure 7). This encodes ethylene-responsive transcription factor ERF113, which is an activator of plant development and stress tolerance pathways, functions downstream of ABA signalling. All other transcripts had lower abundance in the black compared to the orange regions, except for NRT1/ PTR FAMILY 2.11-like, which encodes a high-affinity, proton-dependent glucosinolate-specific transporter. It is involved in the apoplastic phloem-loading of glucosinolates. Several transcripts encoding laccases and peroxidases as well as reticuline oxidases were downregulated in black regions (Figure 7).

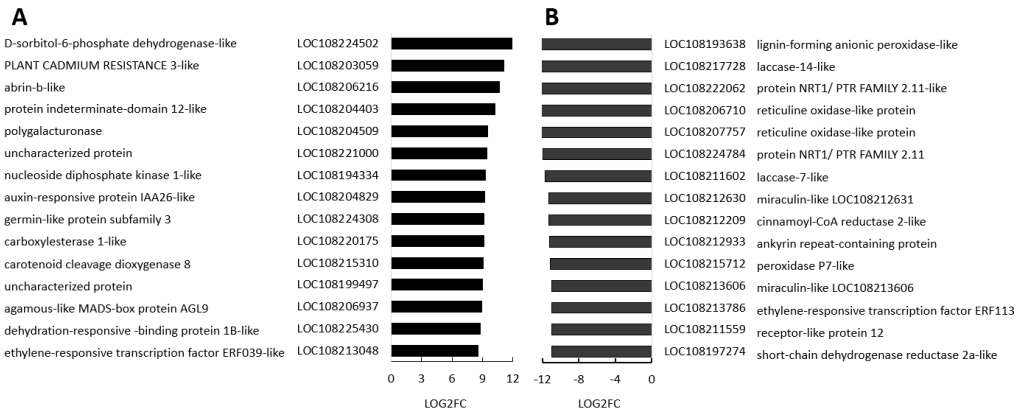

Figure 7. The 15 most increased (A) and decreased (B) transcripts in blackenregions compared to orange regions. Three biological replicates. P-values were calculated using Deseq2 tool and later adjusted using Benjamin-Hochberg correction ($p<0.05$; fold change ≥1).

A number of transcripts were increased in the border regions between the orange and black tissues compared to orange controls (Figure 8). Several of these such as PHYTOCHROME KINASE SUBSTRATE 1, which is a phototropin 1-binding protein required for phototropism are involved in the control of growth. Similarly, levels of transcripts encoding a gibberellin-regulated protein 14 were increased in the border regions. This transcript encodes a GASA domain containing protein, which regulates increases in plant growth through GA-induced and DELLA-dependent signal transduction. The most highly downregulated transcripts in the border regions encode components associated with cell wall metabolism (Figure 8).

Preprints (www.preprints.org) | NOT PEER-REVIEWED | Posted: 5 June 2023 doi:10.20944/preprints202306.0225.v1

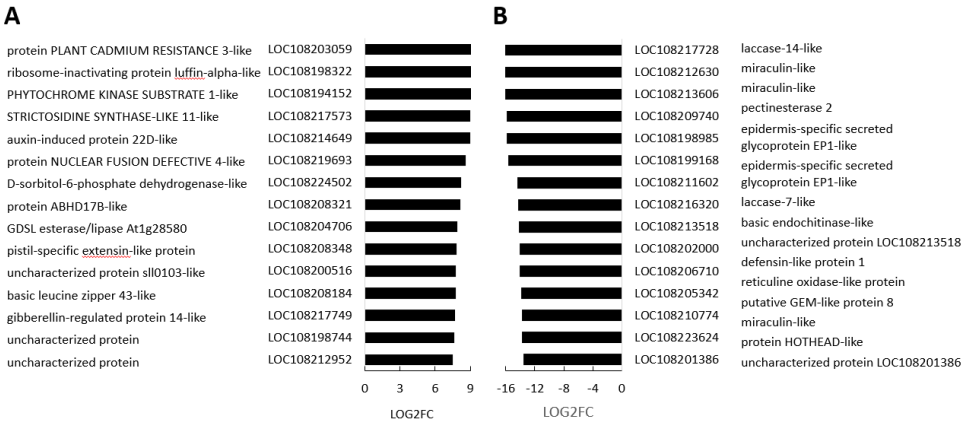

Figure 8. The top 15 most increased (A) and decreased (B) transcripts in border regions compared to orange regions (M/CT). Three biological replicates. Three biological replicates. P-values were calculated using Deseq2 tool and later adjusted using Benjamin-Hochberg correction ($p<0.05$; fold change ≥1).

Of the transcripts that were increased in the black regions compared to border regions (Figure 9), HIP1 encodes an E3 ubiquitin-protein ligase that mediates ubiquitination and subsequent proteasomal degradation of target proteins, and NDR1/HIN1-like protein 12 plays crucial role plant responses to biotic stress. In addition, wound-induced protein 1-like and dormancy-associated protein 1-like were highly expressed in the black regions compared to border regions (Figure 9), as was GLABRA2 Expression Modulator (GEM)-like protein 8 that encodes the GL2-expression modulator, which is involved in the spatial control of cell division, patterning and differentiation in root epidermal cells, and ethylene responsive 8, which is involved in both ABA and immune signaling. Out of cell wall modifying enzymes, a gene encoding pectinesterase 2 was induced in the black regions compared to the border regions (Figure 9). The list of transcripts with significantly lower abundance in the black regions compared to border regions (Figure 9), includes auxin-responsive protein SAUR71-like, which is an early auxin response genes, the bHLH transcription factor bHLH30-like and ERF113, which is involved abiotic stress responses.

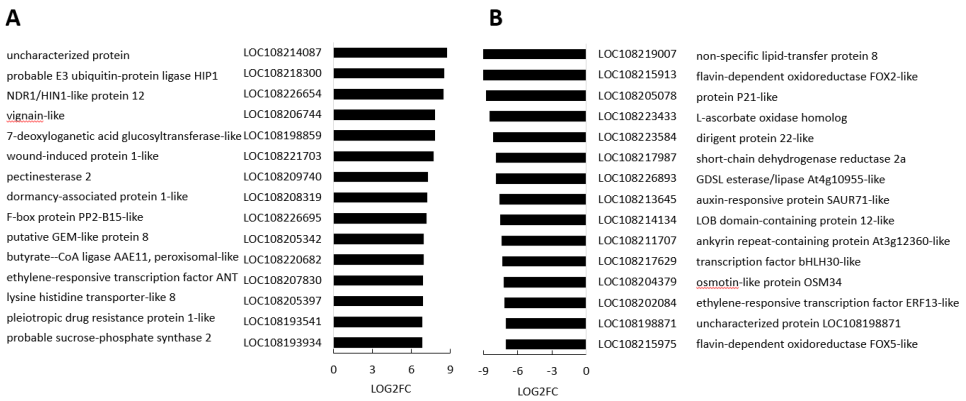

Figure 9. Top 15 most increased (A) and decreased (B) transcripts in black carrot regions compared to border regions (B/M). Three biological replicates. Three biological replicates. P-values were calculated using Deseq2 tool and later adjusted using Benjamin-Hochberg correction ($p<0.05$; fold change ≥1).

3.5. The Metabolic Profiles Are Significantly Changed in Orange and Black Carrot Regions

In total 94 metabolites were identified using HPLC/MS, HPLC and GC/MS analysis of black, border and orange carrot segments. Figure 10 provides an overview of the changes in primary

Preprints (www.preprints.org) | NOT PEER-REVIEWED | Posted: 5 June 2023 doi:10.20944/preprints202306.0225.v1

metabolites observed in the black regions compared to orange regions. The black regions showed a general decrease in primary metabolites, particularly sugars and amino acids. Conversely, increases in the abundance of lysine and γ-aminobutyric acid (GABA) were observed in the black segments. A large decrease in tricarboxylic acid (TCA) cycle intermediates, including fumarate, malate and citrate, was observed in the black regions of the cut carrots, along with a general increase in phenolic compounds (Figure 10). Of the 19 amino acids identified in the black and orange carrot samples using GC/MS, the levels of 16 were significantly decreased in the black compared to the orange samples.

Figure 10. The relative levels of metabolites in the sugar, amino acid and tricarboxylic acid (TCA) pathways in the orange (orange bars) and black (black bars) regions of the carrot batons.

The levels of several amines/polyamines were significantly changed in the orange and black carrot samples (Supplemental Figure S8). In particular, the levels of allantoin and putrescine were increased in the black samples. A decrease in the levels of soluble fructose, glucose, sucrose and inositol was observed in the black carrot samples but the levels of mannose, galactose, glycerol and mannitol were increased compared to the orange regions samples (Supplemental Figure S10). In particular, mannitol was 10 times more abundant in the black than the orange samples. The levels of threonic and galactaric acids were increased in the black samples. Significant increases in the levels of most of the 19 identified fatty acids were observed in the black carrot segments but no significant differences in the major carrot carotenoids were found (Supplemental Figure S11). However, there was a significant decrease in lutein levels in the black compared the orange carrot regions.

There was a general increase in the levels of soluble phenolic compounds in the black carrot segments (Figure 11). In particular, significant increases in the levels of chlorogenic acid, caffeic acid, dicaffeoylquinic acid and 5-caffeoylquinic acid were found. Interestingly, phenylalanine levels were lower in the black regions while many intermediates in the phenylpropanoid pathway and products of the pathway were increased. Moreover, the lignin content of the black regions was more than double that of the orange regions (Figure 11). Differences in lignin composition were observed between the orange border regions and black regions, with S units only present in black regions in

Preprints (www.preprints.org) | NOT PEER-REVIEWED | Posted: 5 June 2023 doi:10.20944/preprints202306.0225.v1

addition to more abundant G and H units (Figure 11). However, there were no dead cells in the samples at the time of harvest.

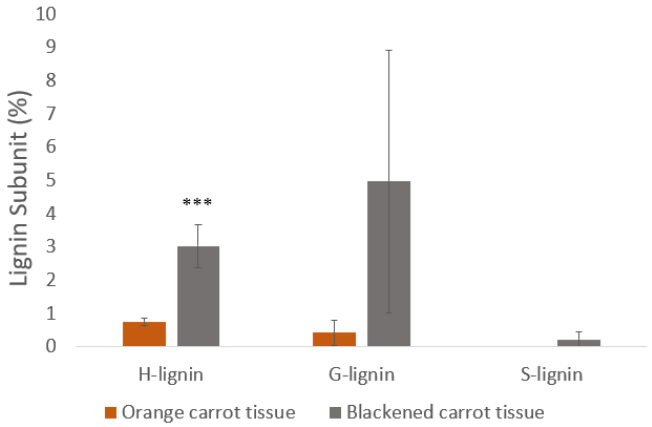

Figure 11. A comparison of the lignin subunit contents of orange and blackened regions of carrot batons (%). The lignin subunits are also known as *p*-hydroxyphenyl (H-lignin), guaiacyl (G-lignin) and syringyl (S-lignin). Data are the mean values ± SD (n = 4). Significant differences between orange and black samples were calculated with a T-test, ***p<0.001. P = 0.0004.

4. Discussion

Post-harvest deterioration of crops is a major contributor to food waste and an important threat to food security. Enzymatic browning is a common cause of the discolouration seen in root vegetables [5]. The data presented here reveals the complexity of transcriptome and metabolome reprogramming that occurs when cut carrots produce black deposits, a process that is slowly induced by wounding only in aged carrots that have been stored for a long period underground. This phenomenon was only observed in mature carrots that are over 1 year old at the point of harvest. The carrots that are 430 days old have a high propensity to show blackening at values twice as high in carrots in younger age ranges. This finding strongly suggests that carrot age or the length of storage underground to prevent sprouting is the major factor that causes susceptibility to blacken. The appearance of black regions in processed carrots followed a similar timescale in carrots harvested from all field sites, the highest level of blackening occurring either on the day of processing or the following day (Schulz, 2021). It is possible that senescence begins in the carrot taproots that have been stored underground for long periods. This process is likely to incorporate cell wall fragmentation and pectin degradation. While the pectic oligosaccharides thus produced might then act as signals there is no evidence in the transcriptome profile of pathogen-like responses upon subsequent wounding.

The data presented here suggest that processing-induced wounding alone does not cause the blackening. Hence, the activation of the wounding response is age-dependent. The blackening process involves substantial reprogramming of gene expression and the activation of secondary metabolism, leading to an accumulation of phenolic compounds and lignin. The accumulation in the black regions of chlorogenic acid (Figure 11), which is widely recognised as a browning substrate in both fruits and vegetables, can be a cause for formation of black deposits.

Differences in the lignin composition of the cells was observed between the black and border regions. Syringol (S) lignin was present only in the black regions in addition to more abundant guaiacol (G) and p-coumarin (*H* unit) type lignin units. The sinapyl alcohol content was previously found to increase during late-stage lignification in carrots, leading to S-lignin accumulation [33]. However, the levels of transcripts involved in processes associated with phenylpropanoid pathway and enzymatic browning were decreased in the black regions, including transcripts encoding enzymes involved in phenylalanine metabolism, glutathione metabolism and the fatty acid degradation pathways. Sine the black cells still appear to be alive and viable, these findings are somewhat surprising given that phenolic compounds closely associated with PPO, including

 doi:10.20944/preprints202306.0225.v1

chlorogenic acid, caffeic acid, and 5-caffeoylquinic acid, were enriched in the black regions. The transcriptome data clearly indicate that the expression of genes involved in secondary metabolism is constrained following the accumulation of secondary metabolites. The rationale for this regulation is uncertain because there has already been extensive accumulation of certain secondary metabolites, e.g. chlorogenic acid, and also lignin. It may serve to prevent a starvation response because of the depletion of primary metabolites in the black carrot regions.

The black carrot regions show a general decrease in primary metabolites particularly amino acids, soluble sugars (glucose, fructose, sucrose) and organic acids. This may be related to the increases in respiration associated with senescence and wounding, together with a diversion of metabolites to phenolic compounds, fatty acids, and other carbohydrates (galactose, mannose, glycerol, and mannitol). The levels of most of the organic acids involved in the TCA cycle were decreased in black carrot regions, indicating a depletion of respiratory substrates. The low levels of glucose, fructose and sucrose also suggest that the black regions were running out of vital carbohydrate reserves. Observed decreases in the aromatic amino acids further support the conclusion that the blackening process involves a switch from primary to secondary metabolism. The dramatic ~8-fold increase in GABA in the black regions is indicative of an abiotic stress response. Increases in other stress-induced signalling metabolites, including allantoin and putrescine, were also observed. A strong correlation between succinic acid and GABA was observed in carbon starvation-induced GABA production in Arabidopsis leaves [34]. Jasmonate (JA) synthesis was increased in wounded lettuce leaves, together with amplified wound signalling through the oxylipin pathway associated with leaf browning [35]. However, the levels of only one transcript associated with JA signalling was increased and there was no evidence of changes in JA synthesis in the black regions.

The cell walls in the black regions were markedly changed with increased lignification accompanied by decreases in the detection of xyloglucan, HG pectin and RG-I pectin. This finding suggests that cell wall degradation was enhanced in the black regions. Aspects of the observed cell wall modulations between the orange, border and black carrot regions may also relate to changes to cell wall structure that in turn influence the access of the antibody probes. For example, the observed autofluorescence of cell walls of black regions, likely reflecting extensive cross-linking of phenolic compounds, may prevent polysaccharide detection. In short, the cell wall immunohistochemistry clearly reports substantial changes to cell walls across the carrot regions. The levels of galacturonic acid, which is the main component of pectin, were lower in the black tissues. The cell walls in the orange tissue are rich with HG pectin with low, medium and high levels of esterification. The cell walls of the orange carrots were also rich in the RG-I pectin sidechains (1-4)-β-D-galactan and (1-5)-α-L-arabinan, with much lower levels detected in the border regions and little to no detection in the black regions. These findings may suggest that pectin is one of the first compounds to be altered or removed when the blackening process is triggered. Pectin-degrading enzymes are commonly secreted by fungal or bacterial plant pathogens to weaken cell walls [8, 36] but they are also produced by plants, for example in fruit ripening after harvesting [11].

The transcriptome profiling analysis showed increases in transcripts involved in phytohormone signal transduction, particularly auxin signalling, as well as ethylene-responsive transcription factors are more abundant in the black regions compared to the orange regions. The black and border regions also showed decreased levels of transcripts involved in ABA-signalling. DEGs encoding key enzymes involved in SA synthesis, such as chorismate synthase aminodeoxychorismate synthase and several chorismate mutases were low in the black and border regions. Other DEGs encoding proteins associated with PCD such as the lesion simulating disease (LSD)-like proteins and accelerated cell death 6-like proteins were also decreased in abundance. However, two LSD-like and three accelerated cell death proteins, which are negative regulators of PCD were more abundant.

Transcripts involved in the turnover and signalling of phytohormones, particularly auxin were enriched in the black and border regions compared to the orange carrot segments. Like other phytohormones auxin plays a key role in the development and dormancy of the carrot taproot. The endogenous levels of auxin, ethylene, cytokinin, ABA and gibberellic acid (GA3) increase in the taproot up to harvest time and subsequently decrease upon harvest (Halloran et al., 2005). The

 doi:10.20944/preprints202306.0225.v1

changes in hormone levels facilitate a short dormancy period after harvest due to preharvest hormonal accumulation. The levels of cytokinin and auxin increase when the dormancy period ends while ABA, ethylene and GA3 levels decrease. The transcriptome profile suggests that auxin levels are high in the black and border regions compared to the cut carrots, implicating auxin in the susceptibility to blackening following processing.

Phytohormones such as JA play a key role in the lignification process because they are involved in the control of secondary metabolism, and the synthesis of phenylpropanoids [37]. The expression of JA-regulated genes, JA-precursors and MYB-type transcription factors is enhanced by auxin [38]. However, there was no evidence of changes in JA synthesis or signalling in the black carrot regions. Auxin signalling is linked to lignification through the induction of ethylene biosynthesis [39]. A lignin deposition phenotype was reported in mutants defective in 2 leucine-rich-repeat receptor-like kinases, which seemingly link cell wall biosynthesis with ethylene production in Arabidopsis. Auxin has also been implicated in the control of senescence but its mode of action and point of interference with senescence control mechanisms remains poorly defined. For example, ARF2, which is a repressor of auxin signalling that positively regulates leaf senescence, functions in the auxin-mediated control of leaf longevity in Arabidopsis [40].

5. Conclusions

In summary, we present a holistic view of the cellular, molecular, and metabolic processes that contribute to the blackening of processed carrots. The age of the carrots at the time of processing is clearly a major factor controlling the susceptibility to blackening, suggesting that storage-induced ageing and/or senescence is a key factor regulating the blackening process. The data presented here implicate ethylene and auxin-related processes in the control of blackening, a syndrome that involves a massive shift from primary to secondary metabolism resulting in lignification and cell wall disruption. The physiological significance of this rewiring of cell physiology is unknown but it may serve to prevent herbivory or pathogen attack. As such, these findings might be integrated into current molecular-regulatory models of ageing/senescence-related plant defence strategies.

Supplementary Materials: The following supporting information can be downloaded at the website of this paper posted on Preprints.org. Supplemental Figure S1 A comparison of carbohydrate (A) and organic acid (B) levels of orange and black regions of the carrot batons (A). Relative concentration was the mean compound (n=17) normalised to the internal standards. Asterisks indicate the statistical significance level: p-value ≤ 0.05 (*), < 0.01 (**), and < 0.001 (***) using ANOVA. Data is the mean +/- standard deviation. Supplemental Figure S2. Heatmap comparison of transcript profiles of orange and border regions (A) and orange and blackened regions in carrot tap roots. Supplemental Figure S3. Define abbreviations: DEG, B_CT, B_M, B_CT, ´BH´ Check the title of the fig, B_CT is listed twice; Supplemental Figure S4. Mentions comparisons of black vs control, black vs middle and middle vs control. I assume that middle should read border? Supplemental Figure S5. Bubble plot for Kyoto Encyclopedia of Genes and Genomes (KEGG) pathways enrichment analysis in black vs. control (A), middle vs. control (B), and black vs. middle (C) comparisons. Supplemental Figure S6. Heatmap of the transcripts encoding polyphenol oxidases and transcripts associated with tyrosine metabolism that were decreased in the border carrot regions. P-values were calculated using Deseq2 tool and later adjusted using B-H method (fold change ≥1). Supplemental Figure S7. Heatmap of the transcripts encoding phytohormone associated pathways that were changed in the black and border regions relative to the orange regions. Log2 transformed mean normalized expression (log2(mean(normalized counts))) of selected hormone-associated genes representing gibberellins (A), abscisic acid and strigolactones (B), and auxins (C) in black (B), middle (M), and control (CT) samples; Supplemental Figure S8. Heatmap of the transcripts encoding transcription factors that were changed in the black and border regions relative to the orange regions. Heat maps of log2 transformed mean normalized expression (log2(mean(normalized counts))) of

selected transcription factors representing WRKY (A), bHLH (B), ERF (C), TCP (D), MYB (E), and GATA (F) families in black (B), middle (M), and control (CT) samples. Supplemental Figure S9. The relative levels of amines/polyamines in orange and black carrot regions. Relative concentrations were calculated as the mean compound (n=17) normalised to the internal standards. Asterisks indicate the statistical significance level: p-value ≤ 0.05 (*), < 0.01 (**), and < 0.001 (***) using ANOVA. Data are the mean +/- standard deviation. Supplemental Figure S10**.** Relative levels of carbohydrates in orange and black carrot samples. Relative concentration was the mean compound (n=17) normalised to the internal standards. Asterisks indicate the statistical significance level: p-value ≤ 0.05 (*), < 0.01 (**), and < 0.001 (***) using ANOVA. Data are the mean +/- standard deviation. Supplemental Table S1. Differentially expressed transcripts with an adjusted *p*-value of less than 0.05.

Author Contributions: Concept, CHF; Methodology, KS, PK, GM, RDH, SRV, RK, PS, AK, BK, CHF; Formal analysis KS; Investigation KS, GM; Resources CHF; Data curation KS BK; Writing -original draft preparation KS, CHF; Writing-reviewing and editing PK, RDH, AK; Supervision: CHF, PK, RDH, AK; Project administration CHF; Funding acquisition CHF.

Data availability statement: Original data are available from the authors upon request. RNAseq data can be found in the repository Sequence Read Archive (SRA) of the National Center for Biotechnology Information (NCBI) under the project number PRJNA966197 and submission number SUB13217137.

Acknowledgments: This research was fundeed by UKRI (BB/R505535/1), a BBSRC CASE studentship for KS with Kettle Produce Ltd (UK).

Conflicts of Interest: The authors declare no conflicts of interest.

References

1. **Taranto, F., Pasqualone, A., Mangini, G., Tripodi, P., Miazzi, M., Pavan, S., Montemurro, C.,** 2017. Polyphenol Oxidases in Crops: Biochemical, Physiological and Genetic Aspects. International Journal of Molecular Sciences **18**, 377.
2. **Queiroz, C., Lopes, M.L.M., Fialho, E., Valente-Mesquita, V.L.,** 2008. Polyphenol Oxidase: Characteristics and Mechanisms of Browning Control. Food Reviews International **24**, 361–375.
3. **Moon, K.M., Kwon, E.-B., Lee, B., Kim, C.Y.,** 2020. Recent trends in controlling the enzymatic browning of fruit and vegetable products. Molecules **25**, 2754.
4. **Glagoleva, A.Y., Shoeva, O.Y., Khlestkina, E.K.** (2020) Melanin pigment in plants: Current knowledge and future perspectives. Front. Plant Sci. 11:770.
5. **Ru, X., Tao, N., Feng, Y., Li, Q. and Wang, Q.,** 2020. A novel anti-browning agent 3-mercapto-2-butanol for inhibition of fresh-cut potato browning. Postharvest Biology and Technology. **170**, 111324.
6. **Mohnen, D.,** 2008. Pectin structure and biosynthesis. Current Opinion in Plant Biology **11**, 266–277.
7. **Cornuault, V., Posé, S., Knox, J.P.,** 2018. Disentangling pectic homogalacturonan and rhamnogalacturonan-I polysaccharides: Evidence for sub-populations in fruit parenchyma systems. Food Chemistry. **246**, 275–285.
8. **Tayi, L., Maku, R.V., Patel, H.K., Sonti, R.V.,** 2016. Identification of Pectin Degrading Enzymes Secreted by Xanthomonas oryzae pv. oryzae and Determination of Their Role in Virulence on Rice. PLoS ONE **11,** e0166396
9. **Cybulska, J., Zdunek, A., Kozioł, A.,** 2015. The self-assembled network and physiological degradation of pectins in carrot cell walls. Food Hydrocolloids **43**, 41–50.
10. **Fries, M., Ihrig, J., Brocklehurst, K., Shevchik, V.E., Pickersgill, R.W.,** 2007. Molecular basis of the activity of the phytopathogen pectin methylesterase. EMBO J. 26, 3879–3887.
11. **Goulao, L.F., Santos, J., de Sousa, I., Oliveira, C.M.,** 2007. Patterns of enzymatic activity of cell wall-modifying enzymes during.
12. **Ferrari, S., Savatin, D.V., Sicilia, F., Gramegna, G., Cervone, F., De Lorenzo, G.,** 2013. Oligogalacturonides: plant damage-associated molecular patterns and regulators of growth and development. Front. Plant Sci. 4. Article 49.
13. **Cheng, S., Yan, J., Meng, X., Zhang, W., Liao, Y., Ye, J., Xu, F.,** 2017. Characterization and expression patterns of a cinnamate-4-hydroxylase gene involved in lignin biosynthesis and in response to various stresses and hormonal treatments in Ginkgo biloba. Acta Physiologia Plantarum **40**, 7.

14. **Chezem, W.R., Memon, A., Li, F.-S., Weng, J.-K., Clay, N.K.,** 2017. SG2-Type R2R3-MYB Transcription Factor MYB15 Controls Defense-Induced Lignification and Basal Immunity in Arabidopsis. Plant Cell **29**, 1907–1926.
15. **Degenhardt, B., Gimmler, H.,** 2000. Cell wall adaptations to multiple environmental stresses in maize roots. J. Exp. Bot. 51, 595–603.
16. **Denness, L., McKenna, J.F., Segonzac, C., Wormit, A., Madhou, P., Bennett, M., Mansfield, J., Zipfel, C., Hamann, T.,** 2011. Cell wall damage-induced lignin biosynthesis is regulated by a reactive oxygen species- and jasmonic acid-dependent process in Arabidopsis. Plant Physiology **156**, 1364–1374.
17. **Mellidou, I., Buts, K., Hatoum, D., Ho, Q.T., Johnston, J.W., Watkins, C.B., Schaffer, R.J., Gapper, N.E., Giovannoni, J.J., Rudell, D.R., Hertog, M.L. and Nicolai, B.M.** 2014. Transcriptomic events associated with internal browning of apple during postharvest storage. BMC Plant Biology. **14**, 328.
18. **Pedersen HL, Fangel JU, McCleary B, Ruzanski C, Rydahl MG, Ralet M-C, Farkas V, von Schantz L, Marcus SE, Andersen MCF, Field R, Ohlin M, Knox JP, Clausen MH, Willats WGT**, 2012. Versatile high-resolution oligosaccharide microarrays for plant glycobiology and cell wall research. Journal of Biological Chemistry **287**, 39429-39438.
19. **Andersen, M.C.F., Boos, I., Marcus, S.E., Kračun, S.K., Rydahl, M.G., Willats, W.G.T., Knox, J.P., Clausen, M.H.** 2016. Characterization of the LM5 pectic galactan epitope with synthetic analogues of β-1,4-d-galactotetraose. Carbohydrate Research **436**, 36–40.
20. **Cornuault, V., Buffetto, F., Marcus, S.E., Crépeau, M.-J., Guillon, F., Ralet, M.-C., Knox, J.P.,** 2017. LM6-M: a high avidity rat monoclonal antibody to pectic α-1,5-L-arabinan. bioRxiv 161604.
21. **Verhertbruggen, Y., Marcus, S.E., Haeger, A., Ordaz-Ortiz, J.J., Knox, J.P.,** 2009. An extended set of monoclonal antibodies to pectic homogalacturonan. Carbohydrate Research, Pectin: Structure and Function **344**, 1858–1862.
22. **Hatfield, R. D.; Grabber, J.; Ralph, J.; Brei, K**., 1999. Using the acetyl bromide assay to determine lignin concentrations in herbaceous plants: Some cautionary notes. J. Agric. Food Chem. 47, 628−632.
23. **Kärkönen A, Tapanila T, Laakso T, Seppänen M, Isolahti M, Hyrkäs M, Virkajärvi P, Saranpää P**. 2014. Effect of lignin content and subunit composition on digestibility in clones of timothy (*Phleum pratense* L.). J Agric Food Chem 62: 6091-6099.
24. **Chang, S., Puryear, J. and Cairney, J.** 1993. A simple and efficient method for isolating RNA from pine trees. Plant Molecular Biology Reporter. **11**, 113–116.
25. **Iorizzo, M., Ellison, S., Senalik, D., Zeng, P., Satapoomin, P., Huang, J., Bowman, M., Iovene, M., Sanseverino, W., Cavagnaro, P., Yildiz, M., Macko-Podgórni, A., Moranska, E., Grzebelus, E., Grzebelus, D., Ashrafi, H., Zheng, Z., Cheng, S.,Spooner, D., Van Deynze, A. and Simon, P.** 2016. A high-quality carrot genome assembly provides new insights into carotenoid
26. **Dobin, A., Davis, C.A., Schlesinger, F., Drenkow, J., Zaleski, C., Jha, S., Batut, P., Chaisson, M. and Gingeras, T.R.** 2013. STAR: ultrafast universal RNA-seq aligner. Bioinformatics. **29**, 15–21
27. **Okonechnikov, K., Conesa, A. and García-Alcalde, F**. 2016. Qualimap 2: advanced multi-sample quality control for high-throughput sequencing data. Bioinformatics (Oxford, England). **32**, 292–294.
28. **Liao, Y., Smyth, G.K. and Shi, W.** 2019. The R package Rsubread is easier, faster, cheaper and better for alignment and quantification of RNA sequencing reads. Nucleic Acids Research. **47**, e47–e47.
29. **Love, M.I., Huber, W. and Anders, S.** 2014. Moderated estimation of fold change and dispersion for RNA-seq data with DESeq2. Genome Biology. **15**, 550.
30. **Bindea, G., Mlecnik, B., Hackl, H., Charoentong, P., Tosolini, M., Kirilovsky, A., Fridman, W.-H., Pagès, F., Trajanoski, Z. and Galon, J.** 2009. ClueGO: a Cytoscape plug-in to decipher functionally grouped gene ontology and pathway annotation networks. Bioinformatics. **25**, 1091–1093.
31. **Machaj, G. and Grzebelus, D.** 2021. Characteristics of the AT-Hook motif containing nuclear localized (AHL) genes in carrot provides insight into their role in plant growth and storage root development. Genes. **12**, 764.
32. **Wickham H** (2016). ggplot2: Elegant Graphics for Data Analysis. Springer-Verlag New York. ISBN 978-3-319-24277-4,
33. **Schäfer, J., Trierweiler, B. and Bunzel, M.** 2018. Maturation-related changes of carrot lignins: Maturation-related changes of carrot lignins. Journal of the Science of Food and Agriculture. **98**, 1016–1023.
34. **Caldana, C., Degenkolbe, T., Cuadros-Inostroza, A., Klie, S., Sulpice, R., Leisse, A., Steinhauser, D., Fernie, A.R., Willmitzer, L. and Hannah, M.A.,** 2011. High-density kinetic analysis of the metabolomic and transcriptomic response of Arabidopsis to eight environmental conditions. The Plant Journal. **67**, 869–884.
35. **Choi, Y.-J., Tomás-Barberán, F.A. and Saltveit, M.E.** 2005. Wound-induced phenolic accumulation and browning in lettuce (Lactuca sativa L.) leaf tissue is reduced by exposure to n-alcohols. Postharvest Biology and Technology. **37**, 47–55.
36. **Bethke, G., Thao, A., Xiong, G., Li, B., Soltis, N.E., Hatsugai, N., Hillmer, R.A., Katagiri, F., Kliebenstein, D.J., Pauly, M., Glazebrook, J.** 2016. Pectin biosynthesis is critical for cell wall integrity and immunity in Arabidopsis thaliana. Plant Cell **28**, 537–556.

37. **Behr M, Pokorna E, Dobrev PI, Motyka V, Guignard C, Lutts S, Hausman JF, Guerriero G.** 2019. Impact of jasmonic acid on lignification in the hemp hypocotyl. Plant Signaling and Behaviour **14**, 1592641.
38. **Wang Y, Mostafa S, Zeng W, Jin B.** 2021. Function and mechanism of jasmonic acid in plant responses to abiotic and biotic stresses. International Journal of Molecular Sciences **22**, 8568.
39. **Hentrich M, Sánchez-Parra B, Pérez Alonso MM, et al.** 2013. YUCCA8 and YUCCA9 overexpression reveals a link between auxin signaling and lignification through the induction of ethylene biosynthesis. Plant Signaling & Behavior. **8**, e26363.
40. **Lim POK, Lee IC, Kim J, Kim HJ, Ryu JS, Woo HR, Nam HG,** 2010. Auxin response factor 2 (ARF2) plays a major role in regulating auxin-mediated leaf longevity, Journal of Experimental Botany **61**, 1419–1430.